Cross correlation between actinic and visible defect inspection tool for extreme ultraviolet lithography

Seongtae Jeong[a], Chih-Wei Lai[b], Seno Rekawa[a], Chris C. Walton[c], Shon T. Prisbrey[c], Jeffrey Bokor[a,d]

[a]Center for X-Ray Optics, Lawrence Berkeley National Laboratory, Berkeley, CA 94720
[b]Graduate Group of Applied Science and Technology, University of California, Berkeley, California 94720
[c]Lawrence Livermore National Laboratory, Livermore, CA 94550
[d]EECS Department, University of California, Berkeley, CA 94720

ABSTRACT

We present recent experimental results from an actinic (operates at the EUV wavelength) defect inspection system for extreme ultraviolet lithography mask blanks. A method to cross-register and cross-correlate between the actinic inspection system and a commercial visible-light scattering defect inspection system is demonstrated. Thus, random, real defects detected using the visible-light scattering inspection tool can be found and studied by our actinic inspection tool. Several defects with sub-100 nm size (as classified by the visible scattering tool) are found with the actinic inspection tool with a good signal to noise ratio. This result demonstrates the capability of the actinic inspection tool for independent defect counting experiments at a sub-100 nm defect sensitivity level.

Keywords: EUV, lithography, mask, defect, actinic

1. INTRODUCTION

Among various schemes proposed as an alternative or successor to optical lithography, extreme ultraviolet lithography (EUVL) has been recognized as one of the leading candidates[1]. EUVL is a reduction imaging scheme based on all-reflective optical elements and 11-14 nm radiation as the light source. The mask architecture that is being pursued for EUVL is a reflective one. A multilayer reflective coating constructed on a robust substrate such as a Si wafer or low expansion glass plate forms the EUVL mask blank and the circuit pattern is defined with patterned absorber on top of the blank.

One of the challenges for the commercial success of EUV lithography is the fabrication of defect-free masks. In EUVL, critical defects that might affect device performance or yield can arise either from defects in the absorber pattern, particles on top of the multilayer coating or from imperfections in the multilayer coating. While Yan, *et al.* have demonstrated techniques for repairing defects in the absorber pattern using a focused ion beam[2], there is no known technique for repair of imperfections in the multilayer coating. Defects can affect the amplitude and phase of the wavefront reflected from the mask and can significantly reduce the process window for printing features[3,4]. For example, when a defect disrupts the multilayer growth, it can induce a significant drop in local reflectivity(opaque defect or amplitude defect). On the other hand, if the multilayer is deposited conformally over a defect residing on the mask blank substrate, the resultant conformal topography induces a localized phase error in the reflected electric field (phase defect). For the 100 nn device generation, the lateral dimension of critical defects on a 4X reduction mask is approximately 80 nm [4,5] ; the density of these critical defects must be on the order of 0.01 defects per cm2 to achieve adequate mask blank yield. The current deposition technology capability (as measured with visible light scattering tools) is approximately 0.05 critical defects per cm^2. The final goal of the EUV program is 0.001 defects/cm^2.

Part of the 19th Annual BACUS Symposium on Photomask Technology
Monterey, California • September 1999
SPIE Vol. 3873 • 0277-786X/99/$10.00

To achieve the required low level of defect density on mask blanks, inspection of produced mask blanks with adequate defect detection sensitivity is an integral part of process development. Because the EUVL mask blank substrate for the reflective Mo/Si or Mo/Be multilayer coating has the form factor similar to that of a standard silicon wafer, optical scattering wafer inspection tools have been used for routine inspection of EUVL mask blanks. These commercial optical inspection tools have a high throughput close to 100 wafers per hour with high sensitivity. Furthermore, the detection sensitivity of these tools is expected to advance as the industry moves into new device generations. The optical scattering detection tool measures the scattering cross section of defects by detecting scattered photons at various collection angles. However, due to a significant difference in optical properties of the multilayer coating at visible and the operating EUV wavelength, it is uncertain whether the visible inspection tool can find all the EUV printable defects. Therefore, at least at the initial developmental stage of multilayer deposition and inspection technology, an actinic (at-wavelength) inspection is desirable to capture all the defects on an EUVL mask blank. An actinic inspection system is expected to help to establish a non-actinic inspection strategy for ultimate commercial use via cross correlation of the EUV response of defects with their optical response. Actinic inspection also *directly* probes the effect of a defect on the reflected electric field and helps to assess its printability.

Actinic inspection of defects on EUVL mask blank has been pursued by several research groups employing different strategies. Inspection via 1x printing on photoresist was pursued by Nguyen *et al* [6]and flood exposure and partial development of the resist-overcoated mask blank has been actively pursued by Spector *et al*[7]. In previous publications[8,9], we reported on an actinic inspection system, referred to as an EUV scanner, based on raster scanning the EUVL mask blank under a focused EUV beam. The EUV scanner system is installed at Beamline 11.3.2 of Advanced Light Source at Lawrence Berkeley National Laboratory. When a focused EUV beam is incident on a defect, the defect induces a reduction in the intensity of the specularly reflected beam (bright field detection) and scattering of photons into non-specular directions (dark field detection). The detector assembly is constructed for simultaneous detection of bright field and dark field signals. For dark field detection, a microchannel plate (MCP) detector is used with a hole at the center to pass the speculary reflected beam. The specularly reflected beam is captured by the bright field detector situated behind the MCP. The small focal spot is formed by imaging an EUV-illuminated aperture using a pair of bendable glancing angle mirrors in a Kirkpatrick-Baez (KB) configuration. The focal spot size can be varied simply by using apertures of different sizes. The smallest spot size we have produced so far is 2.5 μm by 4 μm. The spot size is currently limited by aberrations in the glancing angle incidence optics. Efforts continue to reduce the aberration and improve the spot size. Alternative optical systems are also being considered.

Through experiments with programmed defect samples, it has been demonstrated that the current EUV scanner can detect both amplitude and phase defects with varying topography and lateral dimensions of sub-100 nm[10]. In this paper, we report on successful demonstration of cross registration of the current EUV scanner with an optical scattering inspection tool and an atomic force microscope so that defects found in one tool can be studied with others. We report on the result of correlation between the EUV bright field signal with the size reported by an optical inspection tool. In the initial cross correlation experiment, several defects with sub-100nm lateral dimension measured by the optical inspection tool were successfully detected with the EUV scanner.

II. CROSS REGISTRATION WITH THE OPTICAL SCATTERING INSPECTION SYSTEM

Experiments with programmed defects are useful for calibrating the system sensitivity and for initial system learning due to their well-defined geometry and properties. However, real defects found on EUVL mask blanks generally have irregular shapes.[11] It is expected that the morphology and composition of defects affect both the visible scattering cross section and the EUV response. Therefore, it is of great importance and of practical relevance to study *real* defects using a variety of inspection/metrology tools including the at-wavelength inspection tool, to correlate the results of each inspection tool and ultimately relate the results to printability. In Ref. 11, Burkhart, *et al.* reported successful cross registration among an atomic force microscope (AFM), a scanning electron microscope (SEM), and a high-throughput optical defect inspection tool (KLA Tencor SP1). Thus, once a defect is found using an optical scattering inspection tool that provides its coordinates as well as the scattering cross section, its morphology and

composition can be studied with atomic force microscopy and scanning electron microscopy with compositional analysis capability. In this section, we report a successful cross-registration between SP1 and the EUV scanner. Cross registration of the EUV scanner with non-actinic inspection tools, so that *the same* defect can be studied with a variety of tools, provides important advantages. First, as an at-wavelength metrology tool, the EUV scanner will help to assess the effect of a real defect on the reflected EUV electric field and therefore its printability. Secondly, comparison between the response of the SP1 and the EUV response of a defect will show the degree of correlation between the two inspection tools for the real defects.

Because the throughput of the current EUV scanner is several orders of magnitude lower than SP1, the only realistic approach for cross registration between the EUV scanner and the SP1 is to employ alignment marks at well-defined positions on the mask blank. Since the 150 mm mask blanks currently fabricated at Lawrence Livermore National Laboratory do not have any embedded alignment marks, a diamond scribe was used to create large alignment marks near the center of the sample. A mark as large as 20 μm can be created with only a gentle contact of a sharp regular diamond scribe without generating much debris. These alignment marks can be easily detected in the SP1 and the optical microscope in AFM. As a result, a list of the defects found by SP1 is provided with their optical scattering cross sections and coordinates as well as the coordinates of the alignment marks. The alignment mark created with a diamond scribe shows a very high level of EUV scattering in the dark field as well as a significant reflectivity reduction. Figure 1(a) and 1(b) show the bright field and dark field at-wavelength image of the diamond scribe alignment mark taken with current EUV scanner. The peak dark field signal strength is 29 times the background dark field signal. The high scattering is expected to come from the multilayer damaged by the diamond scribe tip. The background dark field signal arises from roughness in the multilayer and the number of scattered photons captured by the dark field detector is estimated to be 0.4 % of that of the incident beam. Because the alignment mark is large and the signal in the bright field and dark field is rather large, a relatively large EUV beam with a large pixel size can be used to find the alignment mark rapidly. Once two alignment marks are found, the cross registration between the two systems is reduced to a coordinate transform based on the coordinates of the alignment marks in the two coordinate systems. Employing this method, defects can be located with uncertainty less than 100 μm over 150 mm wafer. A further improvement in positioning accuracy is in progress.

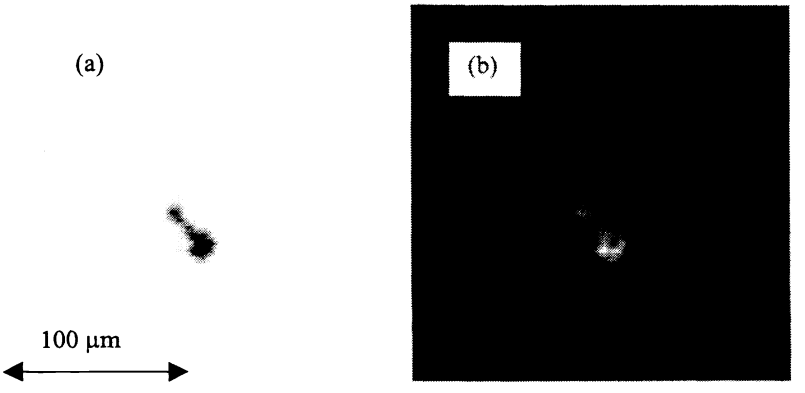

Figure 1. At-wavelength bright (a) and dark field (b) images of the diamond scribe alignment mark are shown. The diamond scribe mark induces significant reflectivity reduction and large scattering.

III. CROSS CORRELATION BETWEEN EUV AND VISIBLE RESPONSE OF DEFECTS.

In an effort to compare the EUV response and visible scattering cross section for a variety of real defects, a total of 35 defects on a Mo/Si multilayer found by the SP1 were scanned in the EUV scanner, following the cross registration method described in the previous section. The sample was a 40 bilayer Mo/Si multilayer fabricated with the low defect density deposition tool at Lawrence Livermore National Laboratory. Figure 2 displays the actinic bright field signal versus the defect size reported by the SP1 for the 35 defects. The

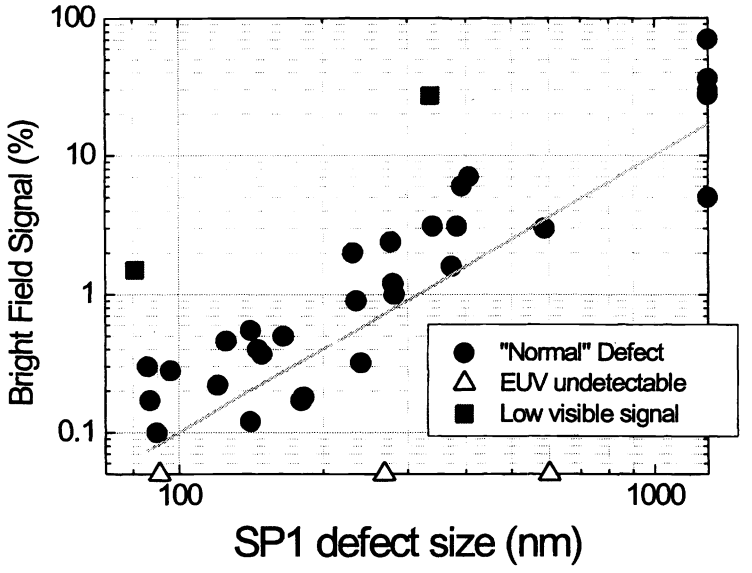

Figure 2. EUV bright field signal is plotted against the size provided by an optical inspection tool, SP1, for 35 defects studied during the cross correlation experiment.

bright field signal is defined as the fractional *reduction* in the number of photons in the bright field region relative to the neighboring clear region. Therefore, the actinic bright field signal represents the amount of light that's taken away from the specular direction due to the defect. The SP1 size represents the diameter of a polystyrene latex (PSL) sphere showing the same amount of scattering of the visible laser radiation as the defect. Three out of those 35 defects were not detectable in the EUV inspection tool. The SP1 size for those defects are 91, 268, and 601nm, respectively and they are shown as open triangles in Figure 2. Possible reasons for the low EUV signal for those defects might be dislocation or detachment of defects during sample transport or that some defects exhibit stronger visible scattering cross section than EUV scattering cross section[12]. There were five defects that the SP1 classified as "area defect". The at-wavelength scanning result of these five defects indicates that they are indeed defects greater than 1 μm in size. These "area defects" are represented with solid circles in Figure 2 on the rightmost axis. The line in Figure 2 is the ratio of the footprint of the defect (essentially square of the SP1 size) to the area of the beam (10 μm^2 for the experiment described in this paper). It is notable that defects represented by solid circles (there are 30 of them shown in Figure 2) fall near the line representing the ratio of the area of the defect to that of the beam. This trend is in good agreement with the assertion that the EUV bright field signal is proportional to the area of a defect and inversely proportional to the area of the probe beam[9]. Therefore, it can be concluded that for a majority of defects studied in this experiment, there exists a *general* correlation between the EUV bright field signal and the SP1 size. In addition, this result can be used for "estimating" the size of the defect from the EUV bright field signal. For example, when a defect displays 1 % change in the bright field, the defect is quite likely to be approximately 200 nm in SP1 size.

In Figure 2, there are two defects displaying rather large departure from the majority of the defects in that their EUV bright field signals are large compared to their SP1 sizes. These two defects are represented as solid rectangles in Figure 2. The SP1 size for these defects are 81 nm and 336 nm and the EUV bright field signal is 1.5 % and 30 %, respectively. Indeed, as is shown in Figure 3, the actinic bright field scan over 336 nm defect reveals an extensive structure with lateral size bigger than 10 μm. The AFM scan (not shown) over the same defect reveals that this is indeed a large defect originating from a crystalline stacking fault in the silicon substrate. The AFM result shows that the lateral size of the defect is greater than 10 μm and its height is 30 nm. The AFM scan (not shown) over the defect with 81 nm SP1 size and 1.5 % EUV bright field signal reveals also that its lateral dimension is 70 nm by 1000 nm and that its height is less than 5 nm. The feature that's common to these two defects showing low visible scattering cross section is that their aspect ratio is very small. This is in good agreement with an independent observation that smooth and

low-aspect-ratio defects (referred to as hillocks) with lateral dimensions in excess of 10 μm and height of a few nanometers are classified as 100 nm defects by visible scattering[13].

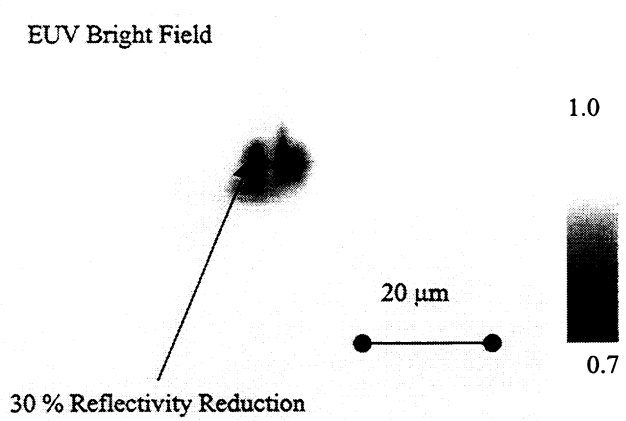

Figure 3. EUV bright field image is shown for defect with 336 nm SP1 size. EUV bright field shows extensive structures with a maximum of 30 % reflectivity reduction at some points.

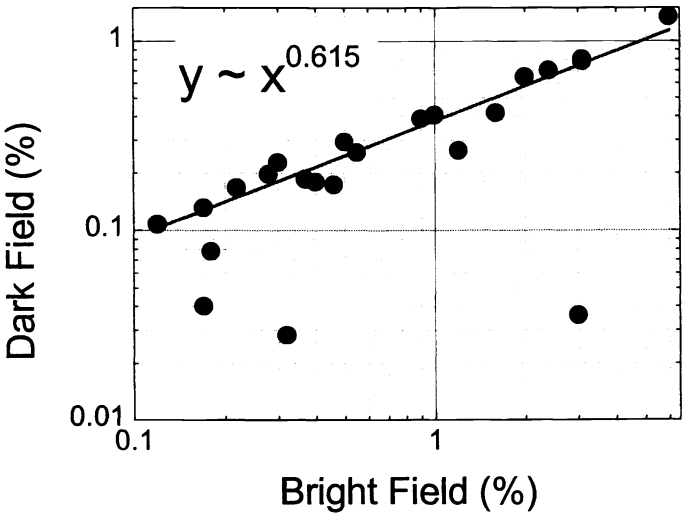

Figure 4. Correlation between the dark field and bright field signals are shown. The dark field signal is defined as the number of photons scattered into the dark field detector divided by the number of photons in the bright field.

In Figure 4, the actinic dark field signal is plotted against the actinic bright field signal for each defect excluding the three defects that were not detectable at EUV wavelength and the five "area" defects. The reason for excluding area defects is that the behavior of the bright field signal and dark field signal becomes complicated when the physical dimension is comparable to the size of the probe beam[9] and mainly we are interested in small sub-μm defects. In Figure 4, the dark field signal is defined as the number of photons that a defect scatters into the dark field detector *divided* by the number of photons captured by the bright field detector. In other words, the dark field signal is scaled to represent the *fraction* of photons in the bright field region scattered into the dark field detector due to the defect. Figure 4 reveals a relatively good correlation between the bright field signal and dark field signal for most of the defects except four. The straight line in Figure 4 is the best-fit power law when the four points are excluded. The good

correlation between the bright field and dark field indicates that for these defects, the bright field signal change is primarily due to scattering of photons out of bright field region into the dark field region. In contrast, when the bright field reduction is dominated by EUV absorption as is the case with opaque programmed defects, the corresponding points tend to lie in the region where the dark field signal is relatively lower compared to the bright field signal. Therefore, comparison between the relative magnitude of the actinic bright field and dark field signal is expected to be useful in differentiating between scattering-dominated defects and absorption-dominated defects and it will be a subject of future research.

In Figure 4, the exponent of the power law-fit is 0.615. If all of the photons scattered out of the bright field detector are detected by the dark field detector, a linear relation is expected between the two signals. In the current detector configuration, however, there is a dead region between two detectors, and the sub-linear dependence can be qualitatively explained by the dependence of the scattering angle on the defect size. For example, a large defect (which shows stronger bright field signal as will be shown later) does scatter photons out of the bright field detector but the scattering angle is so small that some of the photons might not be captured by the dark field detector. One might suspect that the sublinear relation between the two signals might also come from the saturation of the dark field detector at higher signal levels. However, a careful experiment at various incoming beam intensities confirms that the dark field detector (microchannel plate) shows excellent linearity over the range plotted in Figure 4.

Future cross correlation experiments will be performed with samples that have laser scribed alignment marks embedded in the mask blank substrate in order to expedite the cross registration between the different inspection tools. More statistics as shown in Figure 2 and 4 will be compiled for different kinds of defects. For example, defects on top of the multilayer coating might display different behavior compared to defects buried under the multilayer when plotted as in Figure 2 and 4. If that is the case, the information can be used for simple defect classification.

In the cross correlation experiment, there are five defects with sub 100-nm PSL equivalent sizes as shown in Figure 2. An AFM scan (a) of one of those sub-100 nm defects along with its bright field line scan (b) are shown in Figure 5. The line scan shown in Figure 5(b) is an average of ten identical scans to suppress the noise due to the vibration of the beamline optics. The PSL equivalent size of this defect is 86 nm as

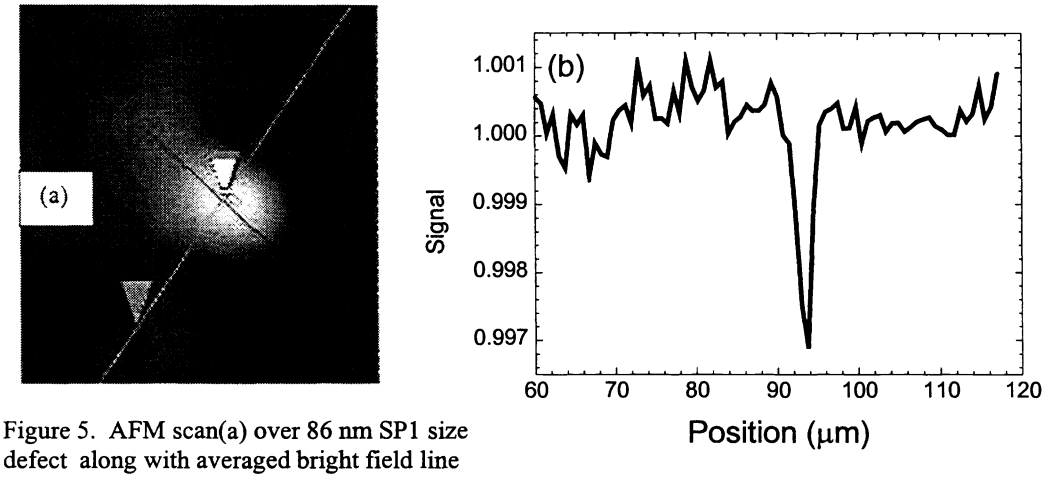

Figure 5. AFM scan(a) over 86 nm SP1 size defect along with averaged bright field line scan (b). The lateral dimension of the defect is less than 100 nm and the height of the defect is 40 nm. The bright field signal induced by this defect is 0.3 %. The residual fluctuations in (b) is the noise due to the beamline optics vibration.

given by the SP1. The dark field signal level indicates that the number of photons scattered by this defect into the dark field is 0.15 % of that of the incident photons. This result confirms that the current EUV scanner can detect defects smaller than 100 nm in lateral size on the mask.

IV. CONCLUSION

We have demonstrated the capability to cross register the current EUV scanner with common inspection and metrology tools in order to detect and characterize real defects on EUVL mask blanks. From initial experiments, it is noted that there exists a general correlation between the PSL equivalent defect size measured by the optical inspection tool and signals in the EUV inspection tools. Furthermore, we have demonstrated a capability to detect defects of sub-100 nm PSL equivalent size in cross correlation experiments. Experiments are planned to continue studying the correlation between the EUV inspection tool and other tools for a variety of defects. Especially, the characteristics of defects showing low visible signal will be studied with a suite of metrology tools.

.ACKNOWLEDGEMENTS

This work is supported by the Extreme Ultraviolet Lithography Limited Liability Company (EUV LLC), the Office of Energy Research, Basic Energy Sciences, of the U.S. Department of Energy under contract No. DE-AC03-76SF00098, SRC contract 96-LC-460 and DARPA grant MDA972-97-1-0010

REFERENCES

[1] See Proceedings of SPIE Vol. 3331, *Emerging Lithographic Technologies II*, Y. Vladimirsky ed., Santa Clara, California, 23-25 February 1998.

[2] P. Yan, S. Yan, G. Zhang, J. Richards, P. Kofron, J. Chow, "EUV mask absorber defect repair with focused ion beam", Proceedings of SPIE Vol 3546, pp206-p213, 18th Annual Symposium on Photomask Technology and Management, Redwood City, California, 16-18 September, 1998

[3] K. Nguyen, PhD dissertation, University of California, Berkeley, 1994

[4] Y. Lin, and J. Bokor, "Minimum critical defects in extreme-ultraviolet lithography masks", Journal of Vacuum Science and Technologies, B **15**(6), 2467-2470, Nov/Dec 1997.

[5] P.Yan, G.Zhang, J. Chow, P. Kofron, J. Langston, H. Solak, P. Kearney, G. Cardinale, K. Berger, and C. Henderson, "EUV mask absorber defect size requirement at 100 nm design rules," *Emerging Lithographic Technologies II*, Proceedings of SPIE Vol 3331, Y. Vladimirsky ed., Santa Clara, California, 23-25 February 1998, pp. 638-645.

[6] K. Nguyen, A. MacDowell, K. Fujii, D. M. Tennant, and L. A. Fetter, OSA TOPS on Extreme Ultraviolet Lithography, Vol 4 pp49, G.D. Kubiak and D. Kania eds., 1996, Optical Society of America.

[7] S. Spector, D. L. White, D. M. Tennant, L.E. Ocola, A. E. Novembre, M. L. Peabody, O. R. Wood II, "A Technique for Rapid At-wavelength Inspection of EUV Mask Blanks", The 43rd International Conference on Electron, Ion and Photon Beam Technology and Nanofabrication, Marco Island, FL, June 1-4, 1999. To be published in Journal of Vacuum Science & Technology B.

[8] S. Jeong, M. Idir, L. Johnson, Y. Lin, P. Batson, R. Levesque, P. Learney, P. Yan, E. Gullikson, J. H. Underwood, J. Bokor, "Actinic detection of EUVL mask blank defects", Proceedings of SPIE Vol 3546, pp524-p530, 18th Annual Symposium on Photomask Technology and Management, Redwood City, California, 16-18, September, 1998

[9] S. Jeong, M. Idir, Y. Lin, L. Johnson, S. Rekawa, M. Jones, P. Denham, P. Batson, R. Levesque, P. Kearney, P. Yan, E. Gullikson, J. H. Underwood, J. Bokor, "At-wavelength detection of extreme ultraviolet lithography mask blank defects", Journal of Vacuum Science & Technology B, **16**(6), 3430-3434, Nov-Dec, 1998.

[10] S. Jeong, L. E. Johnson, Y. Lin, S. Rekawa, P. Yan, P.A. Kearney,E. Tejnil, J.H. Underwood, J. Bokor, "Actinic EUVL mask blank defect inspection system", to be published in *Em erging Lithographic Technologies III*, Proceedings of SPIE Vol 3331, Y. Vladimirsky ed., Santa Clara, California, 14-17 March 1999

[11] S. Burkhart, C. Cerjan, S. Vernon, C. Walton, "Low-defect Reflective Masks for Extreme Ultraviolet Lithography", to be published in *Emerging Lithographic Technologies III*, Proceedings of SPIE Vol 3676, Y. Vladimirsky ed., Santa Clara, California, 14-17 March 1999

[12] Private communication with Edita Tejnil, Intel Corporation.

[13] D. Sweeney, R. Stulen, D. Attwood, and C. Gwyn, "Progres on the development of an EUV lithography system", The 43rd International Conference on Electron, Ion and Photon Beam Technology and Nanofabrication, Marco Island, FL, June 1-4, 1999.